Critical Reynolds Number for a Natural Transition to Turbulence in Pipe Flows

Guy Ben-Dov* and Jacob Cohen†

Faculty of Aerospace Engineering, Technion-Israel Institute of Technology, Haifa 32000, Israel

(Received 8 August 2006; published 6 February 2007)

Experimental results obtained over more than a century have shown that laminar flow in a circular pipe becomes naturally turbulent at a critical Reynolds number of Re $\approx$ 2000. In this Letter a theoretical explanation, based on the minimum energy of an axisymmetric deviation (from the developed pipe flow profile), is suggested for this critical value. It is shown that for Re $>$ 1840 the minimum energy of the deviation, associated with the central part of the pipe, becomes a global minimum for triggering secondary instabilities. For Re $<$ 1840 the global minimum energy deviation is located next to the pipe wall. Previous experimental observations support this explanation.

DOI: 10.1103/PhysRevLett.98.064503 PACS numbers: 47.20.Ky, 47.20.Ft, 47.20.Lz, 47.27.nf

Transition from laminar to turbulent flow in a pipe has been investigated in many studies since the first known experiments by Reynolds [1] (1883). In his experiments Reynolds observed that transition depended on a dimensionless quantity, the Reynolds number $\mathrm{Re} = 2\bar{W}R/\nu$, based on the average (bulk) velocity $\bar{W}$, the pipe radius R and the kinematic viscosity ν. For values of Re above $\approx$ 2000 transition was observed. However, when inlet disturbances were avoided transition could be delayed for Re up to 13 000. In more carefully controlled experiments the Reynolds number for which transition occurs can reach values as high as 10^5 [2]. According to linear stability analysis, the developed pipe flow profile is known to be stable for all Reynolds numbers [3–5].

Nevertheless, in many experiments preformed since the known experiment by Reynolds, transition to turbulence has been observed in the range $1800 < \mathrm{Re} < 2300$. In these experiments either the upstream flow conditions were not carefully controlled, or sufficiently large disturbances were artificially introduced to the flow (e.g., see Refs. [6–10]). Thus, the Reynolds number of $\approx$2000 has been referred to in the literature as the ''critical'' Reynolds number ($\mathrm{Re_{cr}}$) for a ''natural'' transition in pipe flows. Since the linear stability theory, based on infinitesimal disturbances, fails to predict instability, the critical Reynolds number may be theoretically predicted only by introducing finite amplitude disturbances into the flow. Attempts to predict transition by finite amplitude stability have been done in the past (e.g., Refs. [11,12]). Recently finite amplitude solutions of traveling waves have been found to exist in pipe flow for $\mathrm{Re} > \mathrm{Re_{cr}} \approx$ 1250 [13,14], and have been observed in experiments [15]. This $\mathrm{Re_{cr}}$, however, is far from the one known for a natural transition (such low critical numbers were experimentally observed by considering effects of neutrally buoyant suspended particles [16]). To the best of our knowledge a prediction of the known $\mathrm{Re_{cr}} \approx 2000$, based on the instability of finite amplitude perturbations, is absent in the literature.

In this Letter we study the onset of instability of finite amplitude axisymmetric optimal deviations added to the developed pipe flow. The concept of distorting a linearly stable flow by adding finite amplitude deviations to the velocity profile has been used previously for viscous shear flows [17] and for an inviscid free shear flow [18]. The theory of optimal deviations leading to instability of plane channel flows has been presented recently by Bottaro *et al.* [19] and later by Biau and Bottaro [20]. Gavarini *et al.* [21] used this theory to investigate the spatial instability of pipe flows. In the following we, in fact, employ the mathematical method introduced by the latter authors. Through a careful examination of the nonlinear features of this problem we reveal a critical Reynolds number of 1840 associated with the bifurcation between two deviation solutions. This result suggests a possible explanation for the well known critical value for a natural transition to turbulence. Some experimental evidence supporting this outcome is discussed.

The analysis begins with introducing the linearized Navier-Stokes and the continuity equations for small disturbances in an incompressible fluid. A cylindrical coordinate system is used, in which r, θ, and z are the radial, azimuthal, and axial directions, respectively. The equations are solved in nondimensional form, using the centerline base-flow velocity and the pipe radius as characteristic scales, for the base flow of the form $W = 1 - r^2$. The disturbance is assumed to be of the form $\{u(r), v(r), w(r), p(r)\}\exp\{i(\alpha z + n\theta - \omega t)\}$, where u, v, and w are the velocities in r, θ, and z directions, respectively, p is the pressure, α and n are, respectively, the axial and azimuthal wave numbers, and ω is the complex frequency. The equations, together with boundary conditions, constitute an eigenvalue problem for the eigenvalues ω and corresponding eigenfunctions $\{u, v, w, p\}$.

Following Gavarini *et al.* [21], we introduce a variation δW in the base-flow profile which results in variations $\delta\omega$ in the eigenvalue and $\{\delta u, \delta v, \delta w, \delta p\}$ in the eigenfunctions. A variational system is then obtained (see mathematical details in Ref. [22] or in Ref. [21] for spatial analysis). The inner product between the variational system and the adjoint solution of the eigenvalue problem yields

$$i\delta\omega \int_0^1 r(v_a^* u + w_a^* v + p_a^* w)dr = \int_0^1 rG_W \delta W dr, \quad (1)$$

where the subscript a denotes adjoint eigenfunctions, $*$ denotes complex conjugate terms, and G_W is given by

$$G_W = i\alpha(v_a^* u + w_a^* v + p_a^* w) - \frac{1}{r}\frac{d}{dr}(rp_a^* u). \quad (2)$$

Equation (1) is used to find the optimal deviations (the minimum energy deviations added to the base flow and lead to the onset of secondary growing waves). For this purpose a constraint on the magnitude of the deviation $\Delta W = W - (1 - r^2)$ is expressed by the norm [21]:

$$\int_0^1 r\Delta W^2 dr = \epsilon. \quad (3)$$

The resulting problem can be reduced to an unconstrained one, by introducing the Lagrange multiplier λ. The functional to be maximized is then $\mathcal{F} = \omega_i - \lambda(\int_0^1 r\Delta W^2 dr - \epsilon)$, and the condition for optimum is

$$\delta\mathcal{F} = \delta\omega_i - 2\lambda \int_0^1 r\Delta W \delta W dr = 0. \quad (4)$$

Substituting the imaginary part of $\delta\omega$ from (1) into (4) results in a relation which must hold for an arbitrary variation δW. Thus, the optimal deviation is

$$\Delta W = -\frac{1}{2\lambda}\text{real}(\hat{G}_W), \quad (5)$$

where $\hat{G}_W = G_W / \int_0^1 r(v_a^* u + w_a^* v + p_a^* w)dr$. Substituting (5) into (3) yields $\lambda = \pm\frac{1}{2}[\frac{1}{\epsilon}\int_0^1 r\text{real}^2(\hat{G}_W)dr]^{1/2}$, where the plus sign corresponds to a maximization.

The function $\text{real}(\hat{G}_W)$ depends on the base flow W and therefore the deviation ΔW is solved iteratively by employing the algorithm:

$$\Delta W^{j+1} = \Delta W^j - \Omega\left[\Delta W^j + \frac{\text{real}(\hat{G}_W^{j+1})}{2\lambda^{j+1}}\right], \quad (6)$$

where the superscript j denotes the iteration number and Ω is a relaxation parameter. Convergence is reached when the error $\int_0^1 r(\Delta W^{j+1} - \Delta W^j)^2 dr$ is sufficiently small ($\sim 10^{-8}$). The numerical solution of the eigenvalue problem is obtained by the Chebyshev collocation technique, using 80 polynomials.

The above iterative procedure can be used to find optimal base-flow deviations for any Re, n, α, and ϵ. For a specified set of parameters, different functions G_W can be computed with (2), corresponding to different eigenvalues ω of the parabolic profile. Thus, different functions ΔW can be obtained with (5). However, by employing the linear analysis outlined in Eqs. (1)–(5) the resulting solutions are accurate only for infinitesimal deviations. For finite amplitude deviations the iterative procedure in Eq. (6) is employed, where the functions ΔW obtained directly from the parabolic profile may be used as initial guesses. For a sufficiently large ϵ only one deviation solution exists. When ϵ is decreased two solutions may be found (as a result of a bifurcation). As ϵ is further decreased, more bifurcations lead to multiple deviation solutions. In the limit of an infinitesimal ϵ infinite number of optimal deviations exists, corresponding to the infinite number of the parabolic profile eigenmodes.

We solve the optimal deviations for different sets of parameters and find the critical values for which a secondary instability is triggered. The results are restricted to $n = 1$ since in Ref. [21] it has been shown that for a given ϵ these modes become first unstable (see their Fig. 15). For a given deviation the corresponding cross-section energy density (required to generate the distorted profile) is

$$E = 2\pi \int_0^1 r\Delta W[\Delta W + 2(1 - r^2)]dr. \quad (7)$$

Figure 1 presents the cross-section energy density E_n of the optimal deviation required to reach neutrally stable secondary waves (instabilities of the modified base flow), as a function of α for several values of Re. As Re is increased the corresponding curves have lower local minimum energy densities. For $\text{Re} < 600$ a single solution exists (e.g., see the blue solid curve for $\text{Re} = 500$). When Re is increased slightly above $\text{Re} = 600$ a bifurcation occurs, forming two different branches of solutions, indicated by the blue solid and red dashed curves (e.g., see the two curves having two local minima at $\text{Re} = 800$).

Figure 2 presents the optimal deviations corresponding to the minima of the curves shown in Fig. 1. The blue solid lines correspond to the lower $\alpha_{\min}$ branch (blue solid curves in Fig. 1) and the red dashed lines correspond to the higher $\alpha_{\min}$ branch (red dashed curves in Fig. 1). For $\text{Re} > 600$ the deviation associated with the longer secondary wave (blue solid lines) tends to occupy the outer part of the pipe, closer to the wall, whereas the deviation associated with the shorter secondary wave (red dashed lines) occupies the inner part, closer to the centerline. As Re is increased the deviations associated with the longer and shorter secondary waves move further towards the wall and the centerline, respectively.

From Figs. 1 and 2 we note that for Re up to ≈ 2000 the global minimum for each curve is the one located closer to

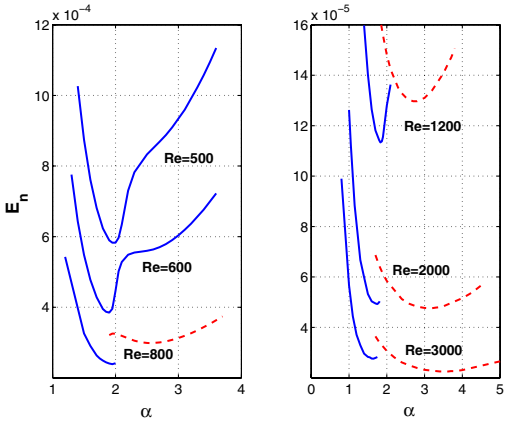

FIG. 1 (color online). Energy density neutral curves vs axial wave-number for various Reynolds numbers.

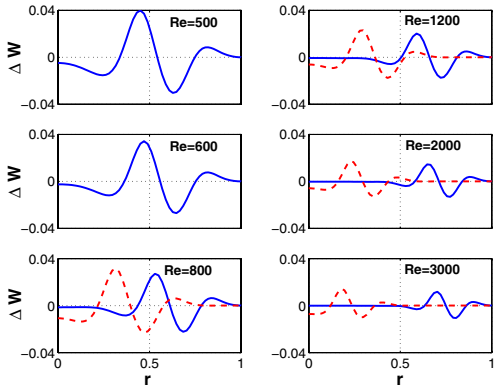

FIG. 2 (color online). Optimal deviation distributions associated with the minima of the E_n curves in Fig. 1. The blue solid lines correspond to the lower $\alpha_{\min}$ branch and the red dashed lines correspond to the higher $\alpha_{\min}$ branch.

the wall, whereas for values above it the global minimum is closer to the centerline. The lowest Re at which the minimum of the higher wave-number deviation solution becomes the global minimum is denoted by Re_m. It is suggested here that Re_m represents the critical Reynolds number ($\mathrm{Re}_{\mathrm{cr}}$) for "natural" transition. This suggestion is discussed below.

In Fig. 3(a) the relation between the minimum disturbance energy density and the Reynolds number is presented for Re = 1200–3000. For all curves in Fig. 3 the blue solid lines correspond to the lower $\alpha_{\min}$ solutions, whereas the red dashed lines correspond to the higher $\alpha_{\min}$ solutions. The intersection of the two lines in Fig. 3(a) is at $\mathrm{Re}_m = 1840$. To explain this intersection it is pointed out that the energy density in (7) consists of two contributions: the first one is $E_d = 2\pi \int_0^1 r\Delta W^2 dr$ representing the energy density due to the external disturbance responsible for the deviation in the profile, whereas the second one, $\Delta E_{\mathrm{int}} = 4\pi \int_0^1 r\Delta W(1 - r^2)dr$, represents the interaction between the deviation and the unperturbed base flow. In Fig. 3(b) their dependence on Re for both branches is shown. The energy E_d associated with the higher $\alpha_{\min}$ branch is lower than the one associated with the lower $\alpha_{\min}$ branch for all Re. This is due to the fact that for a given deviation magnitude the contribution to the energy density is smaller for annular cross sections closer to centerline. Consequently, for a sufficiently large deviation, required to cause an inflectional instability, less energy is needed for a deviation radially closer to the centerline. Similar arguments apply for ΔE_{int}; i.e., the energy ΔE_{int} associated with the higher $\alpha_{\min}$ branch is less negative than the one associated with the lower $\alpha_{\min}$ branch for all Re (the negative sign of ΔE_{int} implies that this part of energy is transferred to the deviation from the parabolic profile). The quantity $-\Delta E_{\mathrm{int}}$ is smaller than E_d. As Re is decreased the magnitude of the deviation required to trigger instability increases and ΔE_{int} becomes more significant. At $\mathrm{Re} < \mathrm{Re}_m$ it reduces the total energy of the deviation next to the wall to a lower value than the energy of the deviation closer to the centerline.

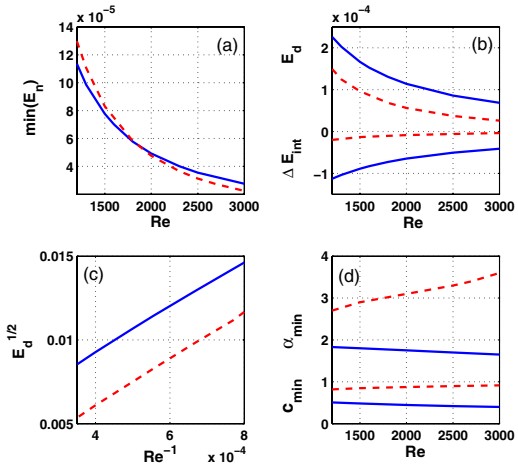

FIG. 3 (color online). (a) Minimum deviation energy density vs Re. (b) Minimal amplitude vs $1/\mathrm{Re}$. (c) Two parts of the energy corresponding to the deviations in (a). (d) phase velocity and axial wave-number corresponding to the deviations in (a).

The scaling of the minimal deviation amplitude (square root of E_d) with Re is $O(\mathrm{Re}^{-1})$ for both solutions as shown in Fig. 3(c). This scaling has been shown to hold for the higher $\alpha_{\min}$ branch in Ref. [21] (their Fig. 14). This result is in accordance with the scaling of $\mathrm{Re}_{\mathrm{cr}}$ for transition found in experiments [23].

In Fig. 3(d) the phase velocity $c_{\min}$ (two bottom curves) and axial wave number $\alpha_{\min}$ (two top curves) corresponding to the two deviation solutions shown in Fig. 3(a), are presented. The figure shows that the subcritical solution (having the minimum energy below Re_m) generates secondary waves which have about twice the wavelength of the supercritical waves (having the minimum energy above Re_m). The time scale $(1/\alpha c)$ of the secondary waves associated with the subcritical solution is approximately 3.5 times longer than the one associated with the supercritical solution. Both the length and time scales of any possible secondary wave solution must be much lower than the axial length and time scales of the deviation (it should be noted that although in the analysis the deviation is independent of the axial coordinate and time, a weak dependence must exist, in order for the deviation to satisfy the Navier-Stokes equations. A discussion on this point is given in Bottaro *et al.* [19]).

Summarizing the main findings, it is claimed that the Reynolds number at which the high wave-number deviation solution becomes the dominant one (having a global minimum energy density), represents the critical Reynolds number for natural transition. Accordingly, natural transition should be characterized with a nonregular motion close to the center of the pipe, the secondary growing waves should be helical, having phase velocities close to 1, and relatively short wavelengths and high frequencies. The latter two characteristics may supply an explanation

for the preference of the solution having a global minimum of energy density above Re_m to be the one leading to transition. If the deviation persists over a sufficiently long time and spatial extent, compared with the respective scales of the secondary waves, these waves can grow and initiate transition.

We now discuss previous experimental results with respect to the above mentioned findings. To the best of our knowledge transition has not been sustained for Re less than ≈ 1750 [10,24]. Measurements of the turbulence level radial distribution in a subcritical case ($Re = 1200$) [7], at which disturbances have been introduced at the pipe inlet where the flow is not fully developed, showed a peak near the wall which decayed with downstream distance. In a different experiment, at which the laminar flow was sustained for high Reynolds numbers [6], large disturbances produced by a ring airfoil in the center of the pipe were observed to lead to turbulence, while smaller axisymmetric disturbances introduced at the inner wall of the pipe by an oscillating sleeve decayed. These two experiments support the above suggested scenario, according to which natural transition begins in the central part of the pipe, whereas for subcritical conditions disturbances are concentrated in the outer part of the pipe and decay with downstream distance.

By introducing large disturbances into the developed flow, experiments showed a well defined turbulent region termed a ''puff'' for $2000 < Re < 2700$ [8,9]. The puffs originated at the pipe centerline, and for $Re > 2000$ the velocity at the centerline dropped significantly. These results are further supporting the above suggested transition scenario. Above Re_m transition is first observed at the central part of the pipe. As expected from the deviation profile, a velocity deficit near the centerline is noticeable (see Fig. 2). Flow visualizations demonstrated that a streamwise helical motion is associated with the puffs [25]. This agrees with the character of the secondary growing waves having $n = 1$. In similar experiments using constant-mass-flux flow [10] the initial three stages of the transition process at moderate Reynolds numbers above 1800 has been described as (a) laminar flow, (b) a gradual reduction of the axial velocity at the center of the pipe, and (c) helical wavelike structures observed in the central axial part of the flow. Additional similar direct-numerical-simulations (DNS) results [26] also support our proposed transition scenario. Very recently it has been shown experimentally that turbulent puffs are sustained only above $Re_{cr} \approx 1750$ [24]. These experiments were followed by DNS results, obtaining $Re_{cr} = 1870$ [27].

The main difference between the on-axis velocity time series (measured close to the disturbance inlet) of disturbances which lead to a puff and those which decay is that the first ones are approximately 50% longer than the latter [10]. Because the time scale of the secondary waves associated with the centerline deviation is much shorter than the one associated with the deviation next to the wall, this experimental observation supports the above mentioned argument that for secondary waves to grow, the deviation has to persist over sufficiently long time and spatial extent.

The authors thank Professor A. Bottaro for a fruitful discussion regarding the method of optimal deviations.

*Present address: University of Illinois at Urbana-Champaign, 1206 West Green St., Urbana, IL 61801, USA. Electronic address: guyb@uiuc.edu

†Electronic address: aerycyc@aerodyne.technion.ac.il

[1] O. Reynolds, Phil. Trans. R. Soc. London **174**, 935 (1883).
[2] W. Pfeniger, in *Boundary Layer and Flow Control*, edited by G. V. Lachman (Pergamon, Oxford, 1961), p. 961.
[3] M. Lessen, G. S. Sadler, and T. Liu, Phys. Fluids **11**, 1404 (1968).
[4] H. Salwen, F. W. Cotton, and C. E. Grosch, J. Fluid Mech. **98**, 273 (1980).
[5] A. Meseguer and L. N. Trefethen, J. Comput. Phys. **186**, 178 (2003).
[6] R. J. Leite, J. Fluid Mech. **5**, 81 (1959).
[7] M. Sibulkin. Phys. Fluids **5**, 280 (1962).
[8] I. J. Wygnanski and F. H. Champagne, J. Fluid Mech. **59**, 281 (1973).
[9] I. Wygnanski, M. Sokolov, and D. Friedman, J. Fluid Mech. **69**, 283 (1975).
[10] A. G. Darbyshire and T. Mullin, J. Fluid Mech. **289**, 83 (1995).
[11] A. Davey and H. P. F. Nguyen, J. Fluid Mech. **45**, 701 (1971).
[12] A. T. Patera and S. A. Orzag, J. Fluid Mech. **112**, 467 (1981).
[13] H. Faisst and B. Eckhardt, Phys. Rev. Lett. **91**, 224502 (2003).
[14] H. Wedin and R. R. Kerswell, J. Fluid Mech. **508**, 333 (2004).
[15] B. Hof, C. W. H. Van Doorne, J. Westerweel, F. T. M. Nieuwstadt, H. Faisst, B. Eckhardt, H. Wedin, R. R. Kerswell, and F. Waleffe, Science **305**, 1594 (2004).
[16] J. P. Matas, J. F. Morris, and E. Guazzelli, Phys. Rev. Lett. **90**, 014501 (2003).
[17] A. E. Gill, J. Fluid Mech. **21**, 503 (1965).
[18] J. Lerner and E. Knobloch, J. Fluid Mech. **189**, 117 (1988).
[19] A. Bottaro, P. Corbett, and P. Luchini, J. Fluid Mech. **476**, 293 (2003).
[20] D. Biau and A. Bottaro, Phys. Fluids **16**, 3515 (2004).
[21] M. I. Gavarini, A. Bottaro, and F. T. M. Nieuwstadt, J. Fluid Mech. **517**, 131 (2004).
[22] G. Ben-Dov, Ph.D. thesis, Technion, Haifa, Israel, 2006.
[23] B. Hof, A. Juel, and T. Mullin, Phys. Rev. Lett. **91**, 244502 (2003).
[24] J. Peixinho and T. Mullin, Phys. Rev. Lett. **96**, 094501 (2006).
[25] P. R. Bandyopadhyay, J. Fluid Mech. **163**, 439 (1986).
[26] H. Shan, B. Ma, Z. Zhang, and F. T. M. Nieuwstadt, J. Fluid Mech. **387**, 39 (1999).
[27] A. P. Willis and R. R. Kerswell, Phys. Rev. Lett. **98**, 014501 (2007).